Please cite this article in press as: Letouzé et al., SDH Mutations Establish a Hypermethylator Phenotype in Paraganglioma, Cancer Cell (2013), http://dx.doi.org/10.1016/j.ccr.2013.04.018

Cancer Cell
Article

SDH Mutations Establish a Hypermethylator Phenotype in Paraganglioma

Eric Letouzé,[1,13] Cosimo Martinelli,[2,3,13] Céline Loriot,[2,3] Nelly Burnichon,[2,3,4] Nasséra Abermil,[3,4] Chris Ottolenghi,[3,6,7] Maxime Janin,[6,7] Mélanie Menara,[2,3] An Thach Nguyen,[2,3] Paule Benit,[8] Alexandre Buffet,[2,3] Charles Marcaillou,[9] Jérôme Bertherat,[3,10,11,12] Laurence Amar,[3,5,12] Pierre Rustin,[8] Aurélien De Reyniès,[1] Anne-Paule Gimenez-Roqueplo,[2,3,4,12,14] and Judith Favier[2,3,14,*]
[1]Programme Cartes d'Identité des Tumeurs, Ligue Nationale Contre Le Cancer, 75013 Paris, France
[2]INSERM, UMR970, Paris-Cardiovascular Research Center (PARCC), 75015 Paris, France
[3]Faculté de Médecine, Université Paris Descartes, 75006 Paris, France
[4]Service de Génétique
[5]Service d'Hypertension Artérielle
Assistance Publique-Hôpitaux de Paris (AP-HP), Hôpital Européen Georges Pompidou, 75015 Paris, France
[6]Service de Biochimie Métabolique, Assistance Publique-Hôpitaux de Paris, Hôpital Necker-Enfants Malades, 75015 Paris, France
[7]INSERM U747, 75015 Paris, France
[8]INSERM U676, Hôpital Robert Debré, 75019 Paris, France
[9]IntegraGen, 91030 Evry, France
[10]Service des Maladies Endocriniennes et Métaboliques, Assistance Publique-Hôpitaux de Paris (AP-HP), Hôpital Cochin, Centre de Référence Maladies Rares de la Surrénale, 75014 Paris, France
[11]INSERM U1016, Institut Cochin, 75014 Paris, France
[12]Rare Adrenal Cancer Network-Cortico Médullosurrénale Tumeur Endocrine, Institut National du Cancer, 75014 Paris, France
[13]These authors contributed equally to this work
[14]These authors contributed equally to this work
*Correspondence: judith.favier@inserm.fr
http://dx.doi.org/10.1016/j.ccr.2013.04.018

SUMMARY

Paragangliomas are neuroendocrine tumors frequently associated with mutations in *RET*, *NF1*, *VHL*, and succinate dehydrogenase (*SDHx*) genes. Methylome analysis of a large paraganglioma cohort identified three stable clusters, associated with distinct clinical features and mutational status. *SDHx*-related tumors displayed a hypermethylator phenotype, associated with downregulation of key genes involved in neuroendocrine differentiation. Succinate accumulation in SDH-deficient mouse chromaffin cells led to DNA hypermethylation by inhibition of 2-OG-dependent histone and DNA demethylases and established a migratory phenotype reversed by decitabine treatment. Epigenetic silencing was particularly severe in *SDHB*-mutated tumors, potentially explaining their malignancy. Finally, inactivating *FH* mutations were identified in the only hypermethylated tumor without *SDHx* mutations. These findings emphasize the interplay between the Krebs cycle, epigenomic changes, and cancer.

INTRODUCTION

Paragangliomas (PGL) are neural crest-derived tumors that arise from parasympathetic ganglia of the head and neck region or from sympathetic ganglia located in the thorax, abdomen, or pelvis. These tumors may develop in the adrenal medulla, in which case they are called pheochromocytomas (PCC) (Lenders et al., 2005). There has been extensive genetic characterization

Significance

Unexpected links between epigenetic and genetic alterations were recently identified with the demonstration that *IDH* mutations impair DNA demethylation in gliomas. Mutations affecting succinate dehydrogenase (SDH), another tricarboxylic acid cycle enzyme, have been identified in several cancers and are particularly frequent in paragangliomas. With this genome-wide analysis of DNA methylation changes in a large paraganglioma cohort, we demonstrate that *SDHx*, and particularly *SDHB*-related metastatic tumors, display a hypermethylator phenotype, associated with downregulation of key genes implicated in chromaffin cell differentiation. These findings explain the oncogenic effect of SDH inactivation and the invasiveness of *SDHB*-mutated tumors and raise the possibility of innovative epigenetic therapies involving DNA demethylating agents for these cancers.

Please cite this article in press as: Letouzé et al., SDH Mutations Establish a Hypermethylator Phenotype in Paraganglioma, Cancer Cell (2013), http://dx.doi.org/10.1016/j.ccr.2013.04.018

of PGL/PCC. At least 30% of patients harbor a germline mutation in one of the ten identified susceptibility genes (Gimenez-Roqueplo et al., 2012): *RET*, *NF1*, *VHL*, *SDHAF2*, *TMEM127*, or *MAX*, and in genes encoding the four subunits of succinate dehydrogenase (*SDHA*, *SDHB*, *SDHC*, or *SDHD*, referred to as *SDHx* genes). Integrated genomic analysis of the largest available cohort of PGL/PCC, recruited by the French COMETE network, identified homogeneous molecular subgroups associated with susceptibility genes (Burnichon et al., 2011) and showed that a large proportion of sporadic PGL/PCC carry a somatic mutation in *VHL*, *RET*, *NF1*, *MAX*, or *HIF2A* genes (Burnichon et al., 2011, 2012a, 2012b; Favier et al., 2012). Overall, 60% of cases harbor a somatic or germline mutation in a known predisposing gene.

Various important issues remain to be unraveled, including the oncogenic role of *SDHx* mutations. Succinate dehydrogenase was the first mitochondrial enzyme to be identified as a tumor suppressor in familial PGL (Baysal et al., 2000). Its inactivation also predisposes to renal cell carcinoma (Ricketts et al., 2008) and gastrointestinal stromal tumors (Janeway et al., 2011). To date, the only mechanism linking SDH to cancer involves hypoxia-inducible factors (HIFs) (Dahia et al., 2005; Gimenez-Roqueplo et al., 2001). SDH dysfunction results in the accumulation of succinate (Pollard et al., 2005), its tricarboxylic acid cycle (TCA) substrate, which acts as a competitive inhibitor of the 2-oxoglutarate (2-OG)-dependent HIF prolyl-hydroxylases (Brière et al., 2005; Selak et al., 2005). This stabilizes HIF-alpha and activates genes that facilitate angiogenesis and anaerobic metabolism. However, the exact role of HIFs in oncogenesis remains unclear (Young and Simon, 2012). Understanding SDH-related tumorigenesis is crucial, because the presence of a germline mutation in the *SDHB* gene is a major risk factor of malignancy and of poor prognosis. Around 40% of all patients with a metastatic form of the disease harbor an *SDHB* mutation (Pasini and Stratakis, 2009). *SDHB*-mutation carriers have a 19-fold higher risk of developing a metastatic disease (Gimenez-Roqueplo et al., 2003) and shorter survival than patients with a malignant PGL/PCC but without *SDHB* mutations (Amar et al., 2007).

DNA methylation changes are hallmarks of human cancers (Hanahan and Weinberg, 2011). Cancer cells often display overall DNA hypomethylation and hypermethylation of promoter CpG islands, resulting in the transcriptional silencing of tumor suppressor genes (Jones and Baylin, 2007). Unlike genetic mutations, DNA methylation is a reversible process and is thus a promising target for drug development (Rodríguez-Paredes and Esteller, 2011). These epigenetic features are also useful as biomarkers for early detection of cancer in blood samples, for prognosis, or for prediction of response to treatment (Laird, 2003). Genome-scale DNA methylation profiling has allowed the identification of epigenetic subtypes in several cancers (Hinoue et al., 2012; Noushmehr et al., 2010). A CpG island methylator phenotype (CIMP), characterized by the concerted hypermethylation of a large number of genes, was initially described in colorectal cancer (Toyota et al., 1999) and was recently identified in glioma (G-CIMP; Noushmehr et al., 2010). In glioma, the G-CIMP phenotype is associated with gain-of-function mutations in *IDH1* and *IDH2* that confer to these enzymes a neomorphic capacity to convert α-ketoglutarate (α-KG, or 2-OG) into the oncometabolite 2-hydroxyglutarate (2-HG). 2-HG acts as a competitive inhibitor of 2-OG-dependent dioxygenases, including histone demethylases and the TET family of 5-methylcytosine (5-mC) hydroxylases, leading to genome-wide DNA methylation alterations (Xu et al., 2011). Succinate also can inhibit these enzymes in vitro, suggesting that SDH-related tumorigenesis may involve epigenetic alterations (Xiao et al., 2012). However, DNA methylation changes of only a limited number of genes have been investigated so far in PGL/PCC (Geli et al., 2008) and have not been compared with expression data or mutational status.

Here, we report the genome-scale methylome and transcriptome profiling of the well-annotated COMETE cohort and investigate the relationship between *SDHx* mutations and DNA methylation changes in a mouse model of SDH-related paraganglioma.

RESULTS

DNA Methylation-Based Classification of Pheochromocytomas and Paragangliomas

We determined DNA methylation profiles of 145 pheochromocytomas and paragangliomas using the Illumina Infinium HM27 DNA methylation assay, which assesses the degree of methylation of 27,578 CpG sites in promoter regions of 14,495 protein-coding genes (Bibikova et al., 2009). Gene expression was previously characterized in most of these samples (Burnichon et al., 2011), and the mutation status of the main genes predisposing to PGL/PCC (*SDHx*, *VHL*, *NF1*, *RET*, *TMEM127*, and *MAX*) was analyzed (Table S1 available online). As previously described (Hinoue et al., 2012), we excluded probes that might be unreliable and probes designed for sequences on sex chromosomes. We selected the 10% most variant probes, according to the standard deviation of the beta values, and performed consensus clustering (Monti et al., 2003) to identify DNA methylation clusters. The optimal classification defined three tumor subgroups (Figure 1A; Figure S1). Tumors of the M1 cluster displayed concerted hypermethylation at a large number of loci (Figure 1B), reminiscent of the CpG island methylator phenotypes described in colorectal cancer and glioblastoma.

For comparison, we applied a second clustering approach, the recursively partitioned mixture model (RPMM; Houseman et al., 2008), to our data set. Cluster assignments using consensus clustering and RPMM were strongly correlated ($p = 9.7 \times 10^{-39}$), with the two methods agreeing on cluster membership for 90% (130/145) of the tumors (Figure S1F). In particular, the M1 cluster was similarly identified by the RPMM approach, with only 1/17 samples misclassified. We based our subsequent analyses on the consensus clusters, which showed better association with clinical criteria.

We next sought to characterize DNA methylation changes in each cluster. We analyzed probes located within and outside CpG islands separately (Takai and Jones, 2002). Most CpGs within CpG islands are demethylated in normal tissues and undergo hypermethylation in tumors (Jones and Baylin, 2007), whereas CpGs outside CpG islands are mostly highly methylated in normal tissues and undergo loss of DNA methylation in cancers (Feinberg and Vogelstein, 1983). Because of the difficulty in obtaining samples of normal adrenal medulla, only three normal controls were available, hence the comparison with tumor clusters had limited power. After FDR adjustment,

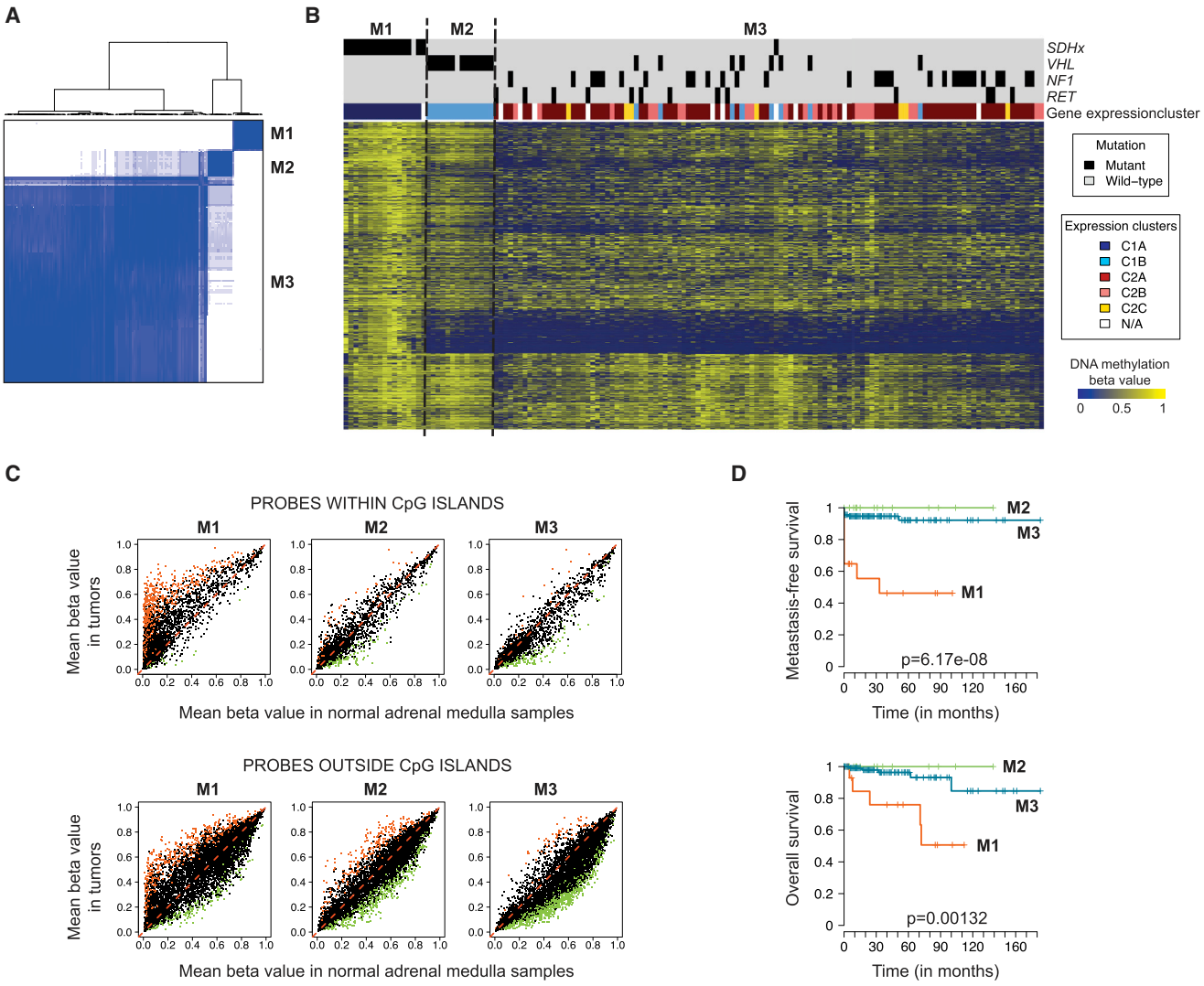

Figure 1. Genome-wide DNA Methylation Profiling of PGL/PCC Identifies a Hypermethylator Phenotype Associated with *SDHx* Mutations

(A) Unsupervised classification of 145 PGL/PCC samples (see Table S1) identifies three stable DNA methylation clusters. The consensus matrix represents the similarity between tumors. Consensus index values range from zero (highly dissimilar profiles, white) to one (highly similar profiles, dark blue). Samples are ordered on the x and y axes by the consensus clustering, which is depicted atop the heatmap. See also Figure S1.

(B) Heatmap representation of DNA methylation profiles. The degree of DNA methylation (beta value) for each probe (row) in each sample (column) is represented with a color scale (dark blue, nonmethylated; yellow, methylated). Tumors are ordered by methylation cluster. Probes are arranged by similarity, as assessed by hierarchical cluster analysis. The mutation status of the main genes predisposing to PGL/PCC (*SDHx*, *VHL*, *NF1*, and *RET*) is indicated above the heatmap, together with expression cluster memberships as determined in a previous study (Burnichon et al., 2011).

(C) Scatterplots comparing methylation levels between tumor subgroups and normal adrenal medulla controls are shown for probes located within (top) or outside (bottom) CpG islands (Takai-Jones definition [Takai and Jones, 2002]). Probes significantly hyper- or hypomethylated in tumors ($p < 0.01$) are indicated in red and green, respectively. See also Table S2.

(D) Kaplan-Meier curves for metastasis-free survival and overall survival.

significant methylation differences between tumors and normal controls were only detected in cluster M1 (1,015 probes with FDR-adjusted $p < 0.05$). However, the number of significant tests ($p < 0.01$) was substantially higher than expected by chance in each cluster (8.7%, 4.8%, and 6.4% in M1, M2, and M3, respectively). Cluster M1 tumors displayed a hypermethylator phenotype, characterized by high methylation levels at a large number of CpG sites, both within (7.2% of probes, $p < 0.01$; Figure 1C; Table S2) and outside (7.0%) CpG islands. Clusters M2 and M3 did not display substantial hypermethylation within CpG islands, but a strong hypomethylation outside CpG islands was observed in both clusters, particularly in cluster M3 (5.9% of probes hypomethylated in M2, 9.6% in M3).

Association with Genomic and Clinical Features

DNA methylation clusters were highly associated with mutational status ($p = 3.3 \times 10^{-33}$) and gene expression clusters ($p = 1.3 \times 10^{-41}$) (Figure 1B; Table 1). In particular, the hypermethylator

Please cite this article in press as: Letouzé et al., SDH Mutations Establish a Hypermethylator Phenotype in Paraganglioma, Cancer Cell (2013), http://dx.doi.org/10.1016/j.ccr.2013.04.018

Table 1. Clinical and Genomic Characteristics of DNA Methylation Consensus Clusters

	Overall (n = 145)	Cluster M1 (n = 17)	Cluster M2 (n = 14)	Cluster M3 (n = 114)	p Value
Gender					
Female	93 (64%)	11 (65%)	6 (43%)	76 (67%)	0.22
Male	52 (36%)	6 (35%)	8 (57%)	38 (33%)	
Age					
Median	44	32	25.5	47	1.80×10^{-7}
Range	7–82	10–63	10–49	7–82	
Histology[a]					
Paraganglioma	15 (10%)	9 (56%)	1 (7%)	5 (4%)	1.51×10^{-9}
Pheochromocytoma	129 (90%)	7 (44%)	13 (93%)	109 (96%)	
Mutational Status					
SDHx	17 (12%)	16 (94%)	0	1 (1%)	3.32×10^{-33}
VHL	21 (14%)	0	13 (93%)	8 (7%)	
NF1	30 (21%)	0	0	30 (26%)	
RET	13 (9%)	0	0	13 (11%)	
Other	64 (44%)	1 (6%)	1 (7%)	62 (54%)	
Expression Cluster[a]					
C1A	16 (12%)	16 (100%)	0	0	1.33×10^{-41}
C1B	22 (16%)	0	14 (100%)	8 (8%)	
C2A	67 (50%)	0	0	67 (64%)	
C2B	22 (16%)	0	0	22 (21%)	
C2C	7 (5%)	0	0	7 (7%)	

Clinical and genomic features are indicated for each DNA methylation cluster, in absolute numbers and as a percentage of each group size. p values are obtained by chi-square tests for qualitative variables and ANOVA for age.

[a]Histology could not be determined for one patient with both abdominal paraganglioma and adrenal pheochromocytoma at first presentation. Gene expression data were available for 134 samples.

phenotype was strongly associated with *SDHx* mutations. In cluster M1, 16/17 tumors were SDH-related (1 *SDHA*, 11 *SDHB*, 1 *SDHC*, and 3 *SDHD* germline mutations), and one was sporadic. Cluster M2 included 13/21 *VHL*-related tumors and one sporadic tumor. All *RET* and *NF1*-related samples were members of cluster M3, together with the remaining sporadic and *VHL*-mutated samples. Clusters M1 and M2 corresponded to the previously described C1A (*SDHx*-related) and C1B (*VHL*-related) expression clusters (Burnichon et al., 2011), and the M3 cluster comprised all tumors of the C2 (*RET*/*NF1*-related) expression cluster, plus eight tumors from the C1B group. Age at diagnosis and histology, which are known to be associated with mutational status (Amar et al., 2005; Neumann et al., 2002), differed significantly between DNA methylation clusters ($p = 1.8 \times 10^{-7}$ and $p = 1.5 \times 10^{-9}$, respectively). The median age at diagnosis was younger for clusters M1 (32 years) and M2 (25.5 years) than for cluster M3 (47 years), and cluster M1 was enriched in paragangliomas (56% versus $\leq$ 7% in clusters M2 and M3). Note that only SDH-related paragangliomas displayed a hypermethylator phenotype. Hypermethylation is thus specifically associated with *SDHx* mutations, rather than a characteristic of extra-adrenal tumors. Methylation clusters were significantly associated with both metastasis-free survival (MFS, $p = 6.2 \times 10^{-8}$) and overall survival (OS, $p = 0.0013$), with the prognosis being much worse for M1 tumors than M2 and M3 tumors (Figure 1D). However, the presence of an *SDHB* mutation predicted prognosis more significantly than methylation cluster membership in our series ($p = 8.9 \times 10^{-10}$ and $p = 8.2 \times 10^{-6}$ for MFS and OS, respectively).

Sdhb Knockout in Mouse Chromaffin Cells Establishes a Hypermethylator Phenotype and Promotes Cell Migration

To investigate the mechanisms linking SDH deficiency with methylation, we generated an immortalized mouse chromaffin cell (imCC) line harboring a complete defect in SDH. We created genetically modified mice in which the endogenous *Sdhb* exon 2 is flanked by LoxP sites, isolated chromaffin cells from their adrenal medulla, and deleted *Sdhb* by Cre-mediated recombination (Figure 2A). Suppression of exon 2 leads to a premature stop codon and to the predicted translation of a truncated 33 amino-acids protein, instead of the 283 amino-acids wild-type (WT) SDHB protein. Two independent *Sdhb*−/− clones were studied (c6 and c8). As previously reported for human tumors (Favier et al., 2009; van Nederveen et al., 2009), *Sdhb*-deficient cells completely lost SDHB protein production but had normal SDHA levels (Figure S2A). They displayed a selective loss of SDH/succinate cytochrome c reductase (SCCR) activity (Figures 2B, S2B, and S2C), accompanied by large increases in both intracellular (Figure 2C) and secreted (Figure S2D) succinate levels and abnormally small amounts of the following organic acids (fumarate and malate) produced by the TCA cycle. Expression and nuclear translocation of HIF2α were also higher than in controls (Figures S2E).

We used reduced representation bisulfite sequencing (RRBS) (Meissner et al., 2005) to examine base-pair resolution DNA methylation patterns in two samples of WT cells and in both *Sdhb*−/− clones. We obtained more than 15 million high-quality aligned reads per sample, yielding quantitative DNA methylation data for 1,530,785 CpG dinucleotides (coverage $\geq$ 10 reads in each sample). Hierarchical clustering identified two clusters corresponding to WT and *Sdhb*−/− cells (Figure 2D). Like SDHx-related tumors, *Sdhb*-deficient cells displayed a widespread hypermethylation both within and outside CpG islands (Figure 2E). We obtained DNA methylation rates with more than ten individual CpG measurements for 78% of CpG islands (n = 12,503). CpG island methylation rates were highly correlated between the two WT samples and between the two *Sdhb*−/− clones (Figure S2F). By contrast, 3,357 CpG islands were significantly hypermethylated, and 242 were significantly hypomethylated in *Sdhb*−/− clones as compared to WT cells (FDR-adjusted $p < 0.05$ and absolute methylation difference > 5%) (Figure S2G). Genes hypermethylated in *Sdhb*-deficient imCCs significantly overlapped those hypermethylated in SDH-related PGL/PCC ($p = 3.2 \times 10^{-170}$), with 1,014 genes in common (Figure 2F; Table S3).

Although SDH-deficiency led to a mean 2-fold decrease in growth rate (Figure S2H), *Sdhb*−/− cells had marked increased migration capacities as assessed in a wound healing scratch assay (Figure 2G). These characteristics are consistent with the known specificities of *SDHB*-related PGL/PCC, which are not associated with increased proliferation but are associated with invasiveness. To investigate the role of DNA methylation in this phenotype, we treated *Sdhb*−/− cells for 72hr with low (10 nM) or higher (5 μM) doses of *5-Aza-2′*-deoxycytidine (decitabine or DAC), an epigenetic modifier that inhibits DNA methyltransferase activity. High doses induced cytotoxicity in all cell types (from 10% to 25% of cell death after 3 days), which was markedly reduced at low doses (cell death <8%). After drug withdrawal, the effect of DAC was assessed on cell proliferation and migration. We observed a dose-dependant blockade of cell growth in both WT and *Sdhb*−/− cells (Figure S2H). In contrast, an inhibition of collective cell migration was specifically observed in SDH-deficient cells, but not in WT cells (Figure 2H).

SDH-Deficient Chromaffin Cells Display Increased 5-mC/5-hmC Ratio and Histone Methylation

Tet-mediated conversion of 5-mC to 5-hmC was evaluated by flow cytometry and immunofluorescence analyses: there was more 5-mC in *Sdhb*−/− than the WT imCCs (Figures 3A and 3B). This effect was reversed by the addition of 2-OG to the culture medium, which also led to an increase in 5-hmC staining of *Sdhb*−/− cells (Figure S3A). The methylation of lysines 9 and 27 of histone 3 was then assessed by western blotting. Loss of *Sdhb* increased H3K9me3, H3K27me2, and H3K27me3 levels (Figure 3C, quantified in Figure S3B). As both H3K9 and H3K27 methylation are closely linked with DNA methylation (Cedar and Bergman, 2009), these effects on histone methylation may contribute to the establishment of the hypermethylator phenotype.

To confirm the inhibition of oxidative demethylation by succinate in human PGL/PCC, we first measured succinate and fumarate concentrations in a subset of tumor samples and confirmed a mean 100-fold increase in succinate levels in *SDHx*- versus non-*SDHx*-mutated PGL/PCC (Table S4). We next used immunohistochemistry to quantify 5-mC and 5-hmC, as well as H3K9me3 and H3K27me3, in 39 paraffin-embedded tumor samples with various genetic backgrounds. All (16/16) *SDHx*-mutated tumors had low 5-hmC levels, whereas 70% (16/23) of non-SDH samples had high levels of 5-hmC (Figure 3D; Table S5). Similarly, 81% of SDH-related PGL/PCC displayed abundant H3K27me3, whereas 43% of non-SDH tumors displayed low H3K27me3 levels (Figure 3E; Table S5). Succinate inhibition of oxidative demethylation by TET proteins and Jumonji domain-containing histone demethylases may thus be the mechanism responsible for the accumulation of DNA methylation in SDH-deficient tumors.

Transcriptional Changes Associated with the Hypermethylator Phenotype

To better understand the impact of DNA hypermethylation in tumors of the M1 cluster, we examined the relationship between methylation and expression changes in these tumors. Principal component analysis indicated that the transcriptome differed between the DNA methylation subgroups (Figure 4A), consistent with the strong association between methylation and expression clusters. Of the 7,136 CpG sites that were differently methylated in M1 and non-M1 tumors (FDR-adjusted $p < 0.05$), 6,850 (96%) were hypermethylated in M1 tumors, resulting in a highly asymmetric volcano plot (Figure 4B). The transcriptome data, available for 134/145 samples, revealed a similar asymmetry (Figure 4C), with 623 genes significantly downregulated (FDR-adjusted $p < 0.05$) and 356 genes significantly upregulated in cluster M1 (Table S6). Integrated transcriptome and methylome analysis revealed that 11.5% of genes with significant hypermethylation in M1 tumors (FDR-adjusted $p < 0.05$ and beta value difference >0.1) also showed more than a 2-fold reduction in gene expression and that the mean shift in expression values correlated with the amplitude of the methylation difference (Figure 4D). To gain a more comprehensive view of DNA methylation changes in M1 tumors, we reanalyzed 22 tumors (ten M1, two M2, and ten M3) using the Illumina Infinium 450K assay, which assesses the methylation levels of more than 485,000 CpG sites. Using probes present on both the 27K and 450K arrays, we verified that the beta value differences between M1 and non-M1 tumors were consistent in the two data sets (mean absolute difference = 0.023). Overall, we identified 4,663 genes with significant hypermethylation of their promoter CpG islands (Table S7). The overlap between the lists of hypermethylated and downregulated genes was highly significant ($p = 1.5 \times 10^{-7}$), with 191 genes showing both significant CpG island hypermethylation and significant downregulation in M1 tumors (Table S8). Gene ontology analysis of this set of genes showed a significant enrichment in terms associated with neuroendocrine differentiation (Table S9). Several genes are associated with catecholamine metabolic process [*PNMT* (Figure S4), *DRD2*, and *SULT1A1*], transport (*SLC6A2*), or secretion (*NPY*); *RET* and *NRP2* are implicated in the differentiation of neural-crest cells. *RBP1* is a tumor suppressor known to be epigenetically silenced in several cancers (Esteller et al., 2002). Downregulation of *SPOCK2*, an inhibitor of matrix-metalloproteases, of *KRT19* (Figure S4), a key marker of the epithelial-to-mesenchymal transition

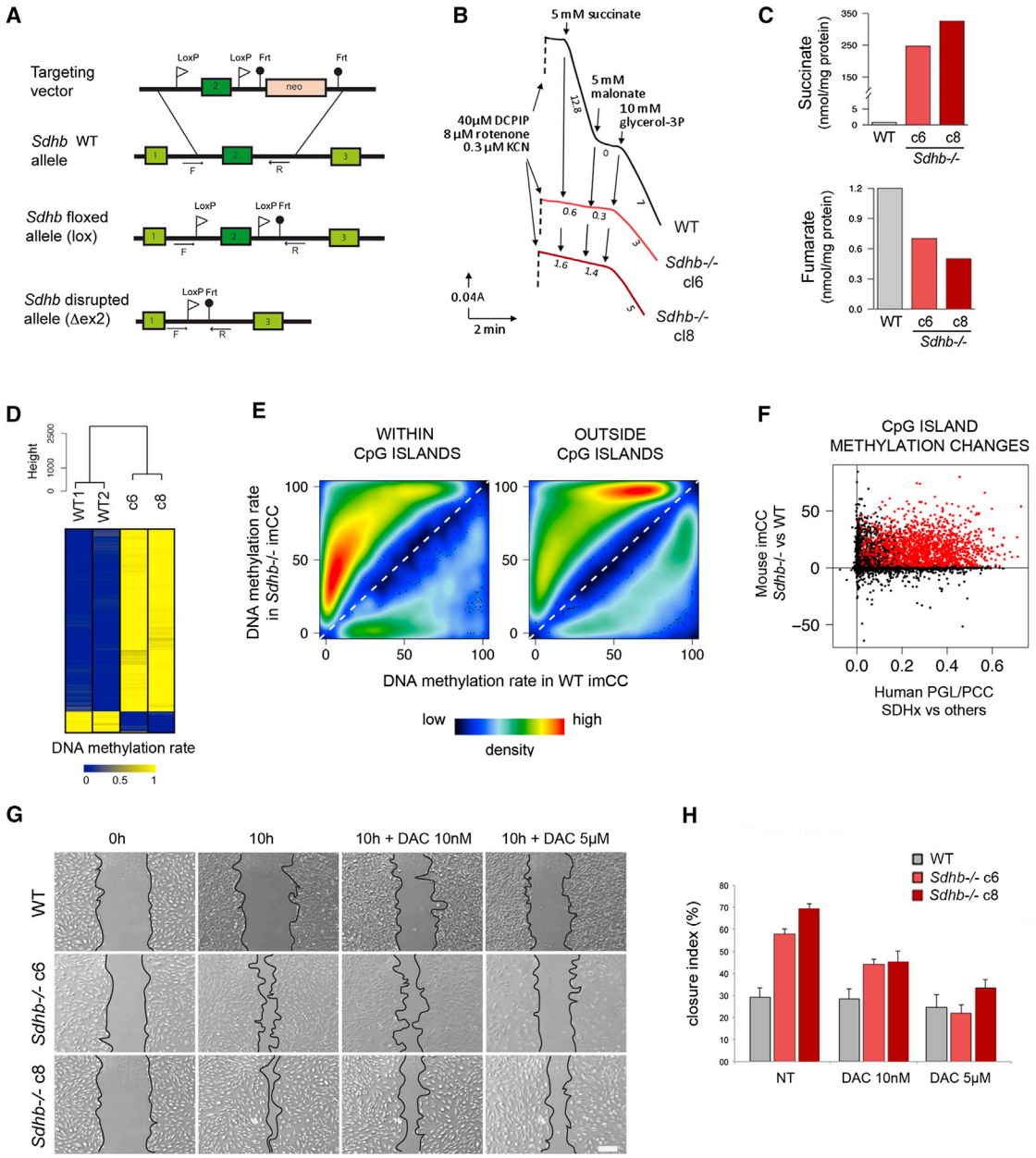

Figure 2. Generation and Characterization of Sdhb-Deficient Mouse Chromaffin Cells

(A) Strategy used for the generation of *Sdhb* knockout in mouse. The targeting vector comprises mouse *Sdhb* exon 2 locus flanked with LoxP sites and followed by a Neomycin (neo) resistance cassette flanked with Frt sites, which is removed after Flip-mediated recombination between the Frt sites. Primers for genotyping (arrows) are indicated below their target sequences.

(B) SDH activity in WT cells (black) measured by 2,6-dichlorophenol-indophenol reduction (in the presence of rotenone, inhibitor of complex I, and cyanide, inhibitor of complex IV) is triggered by succinate addition and subsequently inhibited by adding malonate, a specific SDH inhibitor. The subsequent addition of glycerol-3P triggers the activity of the mitochondrial glycerol-3P dehydrogenase in the same sample. Similar assays were carried out on *Sdhb*−/− c6 (light red) and c8 (dark red) imCCs. Numbers along the traces are nmol/min per mg protein.

(C) Gas chromatography-mass spectrometry analysis of organic acids revealing a substantial accumulation of succinate and the depletion of fumarate in *Sdhb*−/− cells relative to controls.

(D) Hierarchical clustering analysis of DNA methylation profiles from four mouse chromaffin cell samples, with (c6 and c8 clones) or without (WT1 and WT2) a knockout of *Sdhb* gene, analyzed by reduced representation bisulfite sequencing (RRBS). A heatmap indicates the degree of methylation of the 500 most variant CpG sites in each sample (dark blue, nonmethylated; yellow, methylated).

(E) Smoothed color density representation of the scatterplots representing DNA methylation changes between WT and *Sdhb*−/− imCCs, within (left) and outside (right) CpG islands. Only CpG sites showing significantly different methylation rates between WT and *Sdhb*−/− cells are represented.

(F) Comparison of DNA methylation changes in SDH-related human PGL/PCC and *Sdhb*−/− imCCs. CpG island methylation rates were calculated for all mouse/human gene homologs represented in Illumina methylation arrays and RRBS data. Each point represents a gene, with the CpG island methylation difference

(legend continued on next page)

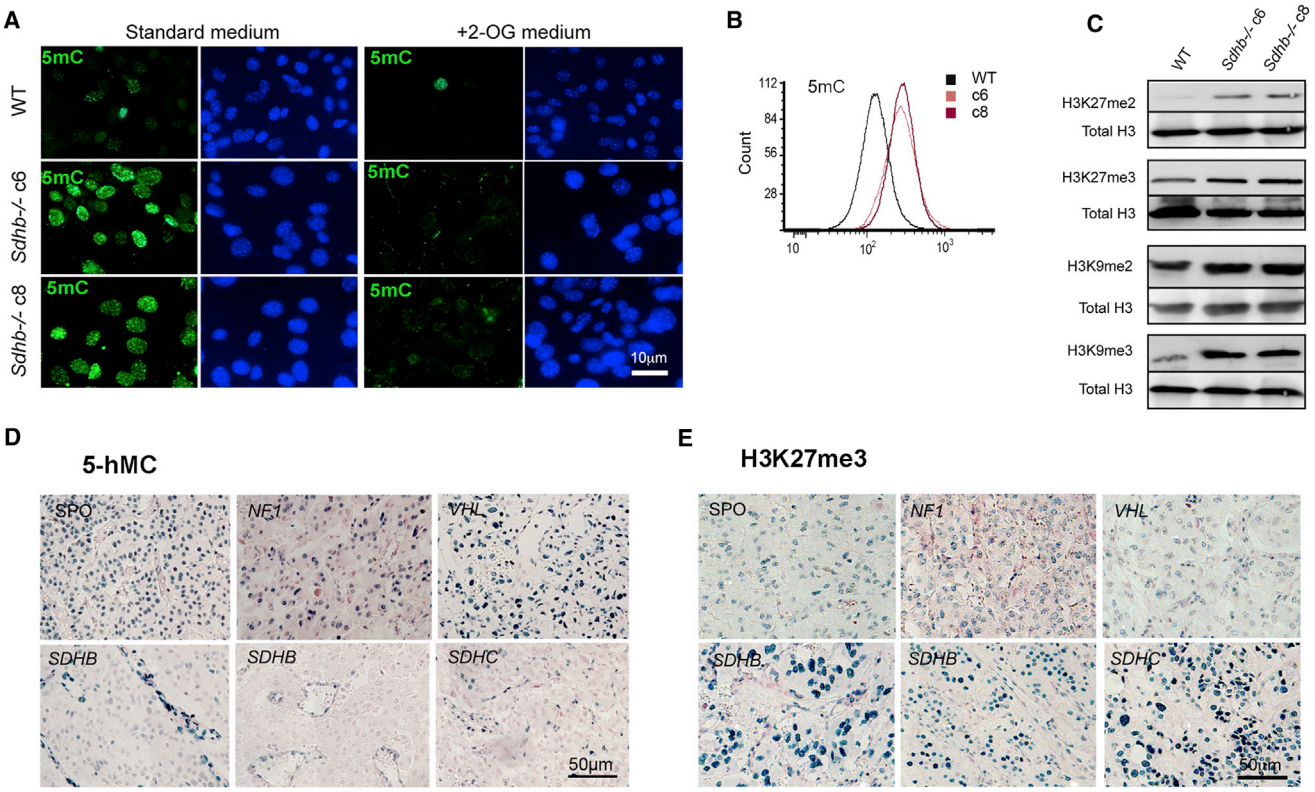

Figure 3. Functional Consequences of SDH Inactivation on Oxidative Demethylation

(A) Immunofluorescence showing a larger number of 5-mC-positive nuclei in *Sdhb*−/− clones. Addition of 2-OG to the culture medium reversed this phenotype. Scale bar = 10 μm.

(B) Fluorescence-activated cell sorting (FACS) analysis also showed that *Sdhb* knockout leads to an increase in 5-mC in imCCs.

(C) Histone lysine methylation levels were assessed by western blotting with specific antibodies. Total H3 was used as a loading control.

(D) 5-hmC levels were studied on human PGL/PCC with various genetic backgrounds. Strong immunostaining of endothelial cell nuclei was observed in all tumor types, whereas the tumor cell staining was weaker in *SDHx*-mutated tumors. Scale bar = 50 μm.

(E) H3K27me3 levels are shown for tumors with various genetic backgrounds. Scale bar: 100 μm; SPO: sporadic tumor. See also Figure S3 and Tables S4 and S5. Scale bar = 50 μm.

(EMT) and of *DNAJA4*, recently shown to be a metastasis suppressor gene (Pencheva et al., 2012), may participate to the invasive phenotype of SDH-deficient cells. These findings indicate that methylome remodeling results in major transcriptional abnormalities in SDH-related tumors, directly associated with their phenotypic characteristics.

Exome Sequencing of the Only Hypermethylated Sample without *SDHx* Mutation Identified Inactivating Mutations in the *FH* Gene

A single tumor in our data set (HS_121) carried no *SDHx* mutation but displayed a hypermethylator phenotype (Figure 1B) as well as both low 5-hmC and high H3K9 and H3K27 methylation (Table S5). This tumor, which also belonged to the C1A (SDH-related) expression cluster was a local recurrence of an adrenal pheochromocytoma resected from a 63-year-old female presenting a high level of urinary normetanephrines. To explain this "SDH-like" phenotype, we performed the whole-exome sequencing of tumor and matched blood DNA. We identified 21 nonsynonymous somatic mutations effecting exons or splice sites in this tumor, 16 of which were predicted to have functional consequences (Table S10). In particular, a somatic mutation was identified in exon 7 of the *fumarate hydratase* (*FH*) gene (c.1043G > C, p.Gly348Ala). This patient also carried a germline mutation in exon 3 of *FH* (c.349G > C, p.Ala117Pro). Both mutations were verified by Sanger sequencing (Figure 5A). The p.Ala117Pro mutation has been described previously in patients with multiple leiomyomatosis and/or renal cancer, displaying reduced FH activity. Interestingly, the patient's clinical record revealed that she had benefited from a total hysterectomy at 35 years old for

between *Sdhb*−/− and WT imCCs along the y axis and the CpG island methylation difference between *SDHx*-related PGL/PCC and other tumors along the x axis. Genes significantly hypermethylated in both human tumors and mouse chromaffin cells are indicated in red.

(G) Cell migration is shown in a wound scratch assay after 10 hr, in standard medium or following 72 hr of DAC treatment at 10 nM or 5 μM. Scale bar = 100 μm.

(H) Reversion of the migratory phenotype by decitabine treatment. Data are mean ± SEM.

See also Figure S2 and Table S3.

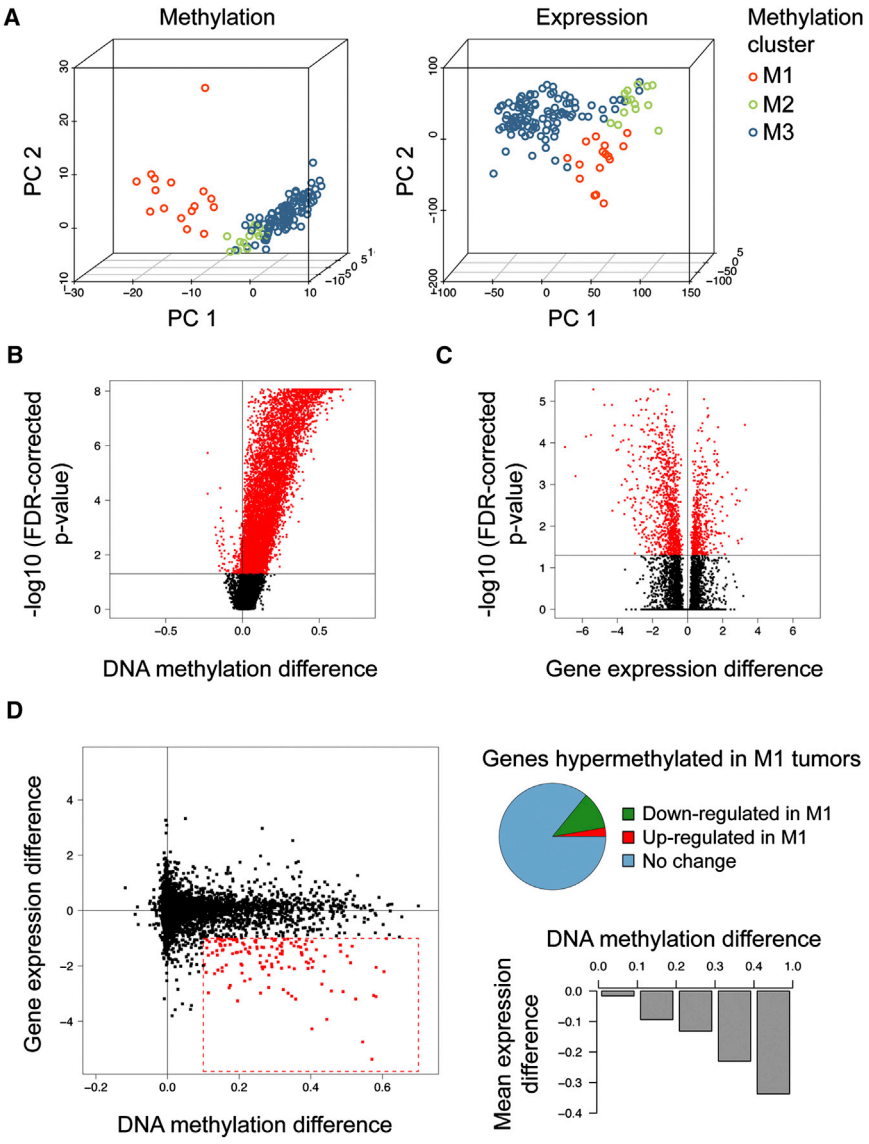

Figure 4. Transcriptional Changes Associated with the Hypermethylator Phenotype in SDH-Related PGL/PCC

(A) Principal component analysis of methylation (left) and expression (right) profiles of PGL/PCC. Tumor samples are plotted in three dimensions using their projections onto the first three principal components (PC). Methylation cluster membership is represented by a color code as described in the legend.

(B) Volcano plot analysis of differentially methylated CpG sites in tumors displaying a hypermethylator phenotype (cluster M1). The beta value difference in DNA methylation between M1 and non-M1 tumors is plotted on the x axis, and the false-discovery rate (FDR)-adjusted significance is plotted on the y axis ($-\log_{10}$ scale). Red indicates probes differing significantly between groups.

(C) Volcano plot analysis of genes differentially expressed between M1 and non-M1 tumors.

(D) Integrated analysis of promoter DNA methylation and gene expression differences between M1 and non-M1 tumors. The starburst plot (left) represents the DNA methylation (x axis) and gene expression (y axis) differences between M1 and non-M1 tumors. Genes that are hypermethylated with a beta value difference >0.1 and have a more than 2-fold decrease in expression levels in M1 tumors are shown as red data points. The pie chart (top right) shows the proportion of hypermethylated genes (FDR adjusted $p < 0.05$ and beta value difference >0.1) that are significantly up- and downregulated in M1 tumors (gene expression difference >1 and <−1, respectively). The histogram (bottom right) shows the mean difference in gene expression levels between M1 and non-M1 tumors as a function of the amplitude of DNA methylation beta value differences. See also Figure S4 and Tables S6, S7, S8, and S9.

hemorrhagic fibromas. The p.Gly348Ala mutation has not been described previously and was predicted to be "probably damaging" by Polyphen software. Tumor HS_121 displayed a selective loss of FH activity (Figure 5B), accompanied by an increase in fumarate concentrations (Figure 5C). Fumarate, like succinate, is a competitive inhibitor of 2-OG-dependent dioxygenases (Xiao et al., 2012), so these findings strongly suggest that FH inactivation causes PGL/PCC by establishing a hypermethylator phenotype.

DNA Hypermethylation and Associated Gene Silencing Are Stronger in *SDHB*-Mutated Tumors

SDHB-mutated PGL/PCC tend to be more malignant than tumors harboring mutations in other SDH subunits (Amar et al., 2005; Pasini and Stratakis, 2009). To determine whether this aggressive behavior is associated with a more severe hypermethylator phenotype, we calculated the mean methylation level across all the CpG sites significantly hypermethylated in M1 tumors and located within CpG islands. This methylation level was, as expected, higher in all M1 tumors than in M2 and M3 tumors (Figure 6A); but, *SDHB*-mutated tumors displayed stronger hypermethylation than other M1 tumors (1 *SDHA*-, 1 *SDHC*-, 3 *SDHD*-, and 1 *FH*-mutated tumors) ($p = 0.0071$). We examined the transcriptional consequences of these differences by calculating the mean expression level of the 191 genes significantly hypermethylated and downregulated in M1 tumors (Table S8). Although these genes were downregulated in all M1 tumors as compared to M2 and M3 tumors, their expression was significantly lower in *SDHB*-mutated tumors than in other M1 tumors ($p = 0.0055$, Figure 6B). The levels of hypermethylation and downregulation of target genes were highly correlated (Pearson's $r = -0.93$, $p = 7.0 \times 10^{-59}$; Figure 6C), suggesting that DNA methylation finely regulates the expression of these genes in PGL/PCC. These findings support the idea that a stronger hypermethylator phenotype, associated with a stronger downregulation of target genes, may participate to the metastatic phenotype of *SDHB*-mutated tumors.

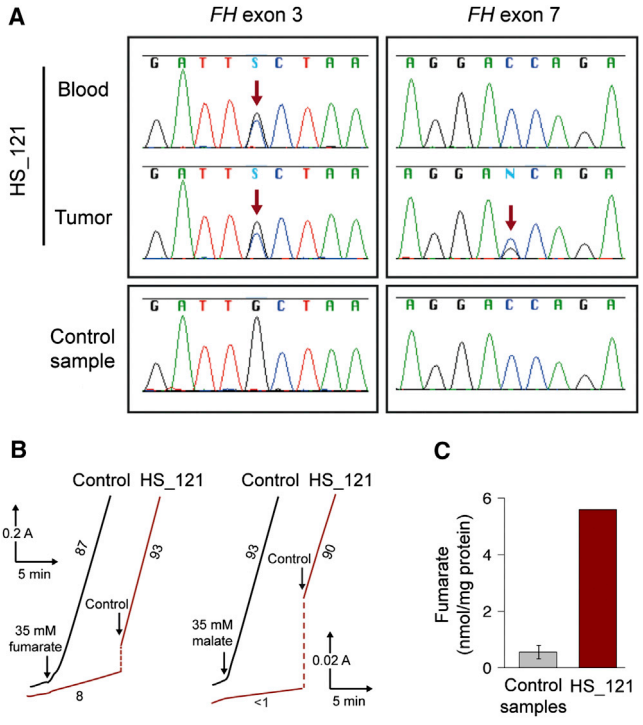

Figure 5. Inactivating *FH* Mutations in the Only Hypermethylated Tumor without *SDHx* Mutation

(A) Sanger sequencing of *FH* gene in DNA extracted from peripheral blood and frozen tumor from patient HS_121 identifies a heterozygous germline mutation (c.349G > C, p.Ala117Pro) in exon 3 and a heterozygous somatic mutation (c.1043G > C, p.Gly348Ala) in exon 7.

(B) Enzymatic activity, assayed spectrophotometrically for the forward (fumarate to malate, left traces) and backward (malate to fumarate, right traces) directions, reveals a severe fumarase deficiency in HS_121 (red) relative to control (black) PGL/PCC samples.

(C) Loss of fumarase activity is associated with a higher fumarate concentration in tumor HS_121 than that in control PGL/PCC (n = 6). For controls, data are mean ± SEM. See also Table S10.

Comparison with the CpG Island Methylator Phenotypes Identified in Colorectal Cancer and Glioblastoma

We investigated whether the hypermethylator phenotype identified in PGL/PCC showed similarities with previously described CIMP phenotypes. We analyzed publicly available data concerning colorectal cancers (Hinoue et al., 2012) and glioblastomas (Noushmehr et al., 2010), obtained with the same Illumina Infinium HM27 methylation array used in this study. For each CpG site, we calculated the mean beta value difference between tumors with and without a hypermethylator phenotype (CIMP-high in colorectal cancer, G-CIMP in glioblastoma). Although we found a significant overlap between hypermethylated loci in the three cancers, the patterns of hypermethylation were particularly similar between PGL/PCC and G-CIMP glioblastomas (Figure 7A). Of 2,241 CpG sites hypermethylated in PGL/PCC of the M1 subgroup (mean beta value difference >0.2 as compared to non-M1 tumors), 847 (38%) were also hypermethylated in G-CIMP glioblastomas, whereas only 279 (12%) were hypermethylated in CIMP-high-colorectal tumors (Figure 7B). Gene set enrichment analysis (GSEA) confirmed that the set of genes hypermethylated in PGL/PCC was more significantly enriched in genes hypermethylated in G-CIMP glioblastomas (enrichment score = 0.75) than genes hypermethylated in CIMP-high-colorectal cancers (enrichment score = 0.47) (Figure S5). Seventeen of the 191 genes epigenetically silenced in PGL/PCC were significantly hypermethylated and downregulated in glioblastoma (including *PNMT* and *RBP1*); 21 were hypermethylated but without significant downregulation (like *KRT19*); and 119, like *NPY*, were not found to be hypermethylated in glioblastoma (Table S8). The similarity between PGL/PCC and glioblastoma hypermethylator phenotypes may reflect the preferential activities of the 2-OG-dependent demethylases inhibited in these two cancers.

DISCUSSION

Metabolic reprogramming in cancer has long been regarded as an indirect response to cell proliferation, but recent evidence has shown that metabolites themselves can be oncogenic by altering several cellular processes (Ward and Thompson, 2012). The oncometabolite 2-HG, produced by mutated IDH enzymes, establishes the G-CIMP phenotype in glioma by inhibiting DNA and histone demethylases (Xu et al., 2011). Succinate and fumarate can activate the oncogenic HIF pathway by inhibiting HIF prolyl-hydroxylases (Brière et al., 2005; Selak et al., 2005). Here, we demonstrate that succinate accumulation in SDH-deficient PGL/PCC establishes a hypermethylator phenotype, by inhibiting 2-OG-dependent oxidative demethylation. Besides, we describe a specific model of SDH-related PGL/PCC, generated by knocking out *Sdhb* gene in chromaffin cells. In the past, the lack of an appropriate cellular model has opposed severe limitations to the understanding of SDH-related oncogenesis. Our model displays a complete inactivation of SDH activity, which cannot be achieved by siRNA-mediated gene silencing, and will be a crucial tool for deciphering the consequences of SDH inactivation in these cells. Our study also led to the identification of a case of *FH* germline mutation in an apparently sporadic PCC displaying a hypermethylator phenotype. *FH* mutations are known to predispose to hereditary leiomyomatosis and renal cell cancer (Tomlinson et al., 2002) but have never been described in PGL/PCC. Altogether, these findings shed light on a novel pathway explaining the tumor-suppressive role of SDH and FH and, echoing the role of *IDH* mutation in glioma, emphasize the link between TCA cycle dysfunction and epigenomic alterations in cancer. Gastrointestinal stromal tumors, renal cancer, and leiomyomas harboring *SDH* or *FH* mutations may also display epigenetic reprogramming, which should be assessed in future DNA methylation studies.

Many cancer-specific hypermethylation events occur in promoter regions of genes that are not normally expressed and are therefore not affected by DNA methylation changes (Widschwendter et al., 2007). To distinguish DNA methylation events of potential functional significance (“driver events”) from these “passenger events”, we integrated the DNA methylation data with gene expression profiles of the same tumors. Only 11.5% of genes with significant promoter hypermethylation in PGL/PCC of the M1 subgroup were underexpressed in these tumors. This is consistent with previous reports in colorectal cancer (7.3%; Hinoue et al., 2012) and glioblastoma (17%; Noushmehr

Please cite this article in press as: Letouzé et al., SDH Mutations Establish a Hypermethylator Phenotype in Paraganglioma, Cancer Cell (2013), http://dx.doi.org/10.1016/j.ccr.2013.04.018

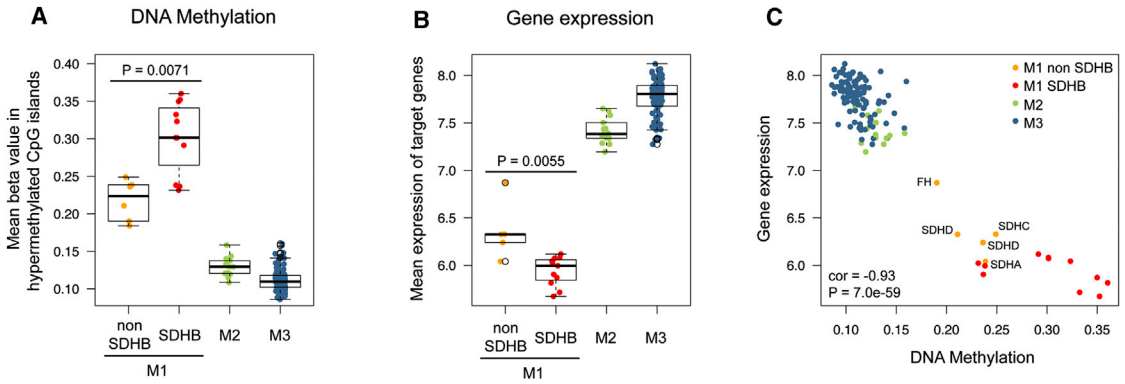

Figure 6. The Hypermethylator Phenotype Is Particularly Severe in *SDHB*-Mutated Tumors

(A) Mean methylation of all CpG island probes significantly hypermethylated in M1 tumors, according to tumor subgroup. Box-and-whisker plots show the distribution of mean beta values relative to each DNA methylation subgroup. M1 tumors are separated into *SDHB*-mutated and *SDHB*-wild-type tumors. The middle bar, median; box, interquartile range; bars extend to 1.5 times the interquartile range.

(B) Mean expression of genes significantly hypermethylated and downregulated in M1 tumors, according to tumor subgroup.

(C) Distribution of mean expression levels of target genes relative to the mean methylation levels of CpG sites hypermethylated in M1 tumors. Tumor subgroups are represented with a color code, and the mutations of non-*SDHB*-mutated M1 tumors are indicated next to each dot.

et al., 2010). Thus, most hypermethylated CpG sites appear to be silent consequences of the inhibition of DNA demethylases, with no evident functional impact. We were however able to show an overall correlation between the level of hypermethylation and downregulation of gene expression. In particular, we identified 191 genes that showed significant hypermethylation and downregulation in M1 tumors and whose expression was closely correlated with the degree of DNA methylation.

Two of the genes showing the strongest evidence for epigenetic silencing in hypermethylated PGL/PCC are, respectively, involved in the differentiation of chromaffin cells (*PNMT*; Eisenhofer et al., 2011) and the epithelial-to-mesenchymal transition (*KRT19*; Moreno-Bueno et al., 2006), which was recently identified as the first mechanistic clue to explain the particularly invasive phenotype of *SDHB*-related tumors (Loriot et al., 2012). The *PNMT* gene encodes the phenyl-ethanolamine-N-methyltransferase, a key enzyme of chromaffin cell metabolism, which catalyzes the conversion of noradrenaline to adrenaline. Reduced *PNMT* expression has been reported in SDH-related tumors, leading to an immature catecholamine secretory profile with predominant secretion of noradrenaline or dopamine (Burnichon et al., 2012b; Eisenhofer et al., 2001). Our findings reveal that *PNMT* is hypermethylated in SDH-related tumors, together with four other genes implicated in catecholamine metabolism (*DRD2*, *SULT1A1*, *SLC6A2*, and *NPY*). Epigenetic regulation is thus a previously unsuspected mechanism explaining the dedifferentiated phenotype of this subgroup of PGL/PCC. Another target of the PGL/PCC hypermethylator phenotype, *RBP1*, is also epigenetically silenced in G-CIMP gliomas (Noushmehr et al., 2010) and several cancer cell lines and primary tumors (Esteller et al., 2002). RBP1 is involved in retinoic acid signaling, leading to loss of cell differentiation and tumor progression (Farias et al., 2005) and may thus have a tumor-suppressive role in PGL/PCC. Studies aimed at elucidating the functional consequences of epigenetic gene silencing will undoubtedly improve our understanding of the role of DNA hypermethylation in PGL/PCC tumorigenesis.

SDH- and VHL-related tumors were previously shown to have similar gene expression features, like the activation of hypoxia-related genes (Dahia et al., 2005). In the COMETE cohort, we showed that, although close, these tumors were classified in two separate gene expression clusters (C1A and C1B) (Burnichon et al., 2011). Here, we found that 150 out of 344 genes (44%) significantly downregulated in SDH- as compared to VHL-tumors were hypermethylated (data not shown). Epigenetic remodeling thus explains a significant part of transcriptional differences between SDH- and VHL-related tumors.

SDHB mutations confer a much worse prognosis than mutations in other *SDHx* genes (Amar et al., 2007). No mechanism has been proposed to explain these differences. We found that although all *SDHx*-mutated tumors displayed a hypermethylator phenotype, the level of hypermethylation was significantly higher, and the expression of target genes was significantly lower in *SDHB*-mutated tumors. As target genes include genes implicated in neuroendocrine differentiation and epithelial-to-mesenchymal transition (EMT), this may explain the particular malignancy of *SDHB*-mutated tumors. *SDHB* encodes a catalytic subunit of SDH (Rutter et al., 2010). We hypothesize that SDH inactivation may be more complete in *SDHB*-mutated tumors than in tumors harboring mutations in other subunits, leading to a higher succinate accumulation and hence to a stronger inhibition of 2-OG-dependent demethylation. However, we were not able to detect significant differences in succinate concentrations between *SDHB*-mutated and other SDH-related tumors. Future studies will be needed to dissect the functional impact of mutations affecting different SDH subunits.

There have recently been several promising findings for epigenetic cancer therapy. Notably, Tsai et al. (2012) demonstrated that low doses of the DNA demethylating agents, DAC and azacitidine, had durable antitumor effects on hematological and epithelial tumor cells. Thus, low doses may help avoid the extreme toxicities of these agents at high dose that have prevented the investigation of the true clinical responses. We show

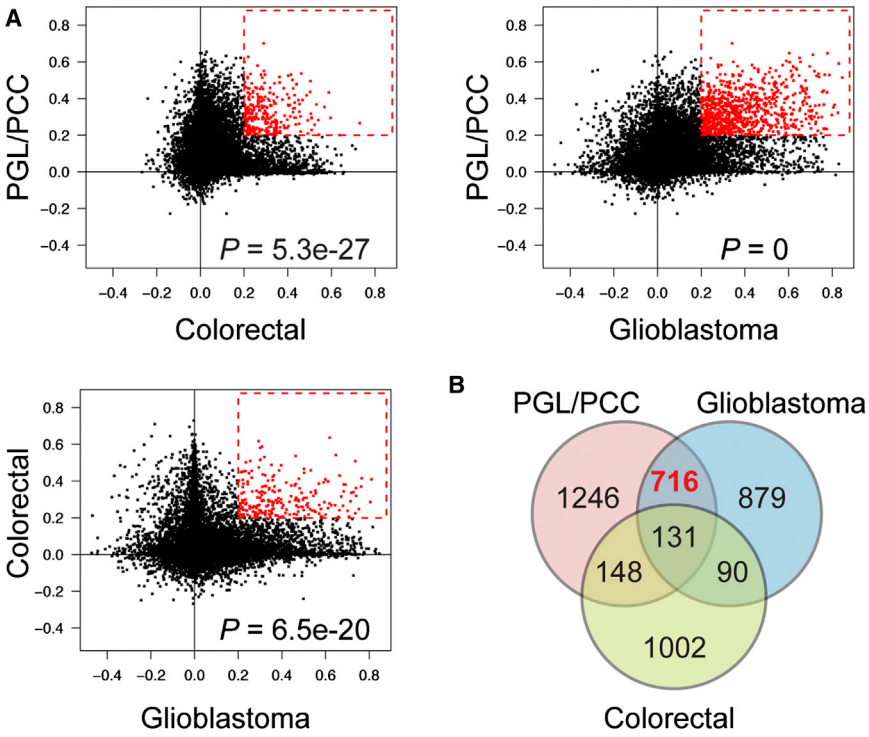

Figure 7. Comparison of Hypermethylator Phenotypes in PGL/PCC, Colorectal Cancer, and Glioblastoma

(A) Correlation between CIMP-specific hypermethylation patterns in the three cancers. The mean beta value difference between CIMP and non-CIMP tumors was calculated for all CpG sites in each cancer type. Each scatterplot represents the correlation of beta value differences between two cancers. Red dots indicate CpG sites hypermethylated in the CIMP subgroups of both cancers (beta value difference >0.2 between CIMP and non-CIMP tumors).

(B) Venn diagram showing hypermethylated loci shared by the PGL/PCC hypermethylator phenotype, the colorectal cancer CIMP-high phenotype, and the glioblastoma G-CIMP phenotype. See also Figure S5.

that the increased migratory capacities of *Sdhb*−/− mouse chromaffin cells are repressed by transient DAC treatment, even at a 10 nM concentration, which led to minor cytotoxicity. The precise molecular changes associated with these treatments will have to be deciphered in future studies, both in vitro and in vivo. In view of these findings, the reversal of promoter DNA hypermethylation and associated gene silencing may rise as an attractive alternative approach to surgery for *SDHx*- and *FH*-mutated PGL/PCC. *NPY*, which shows the strongest transcriptional silencing in M1 tumors, may be a good marker. NPY levels were shown to be increased in the plasma and tumors of patients with PCC and to be significantly lower in extra-adrenal tumors (deS Senanayake et al., 1995). A comprehensive study of candidate markers in a large independent cohort will be useful to determine the best marker of this aggressive subgroup.

In summary, our analysis indicates that PGL/PCC can be classified into three distinct subgroups according to genome-scale DNA methylation changes. The identification of a hypermethylator phenotype in *SDHx*- and *FH*-mutated tumors helps in explaining both the tumor-suppressive role of these genes and some of the phenotypic characteristics of these tumors. The malignancy of *SDHB*-mutated PGL/PCC may be due to a severe epigenetic silencing of genes involved in cell differentiation and EMT. These findings have clinical implications for PGL/PCC diagnosis and may lead to targeted epigenetic treatment for patients with TCA cycle alterations.

EXPERIMENTAL PROCEDURES

Collection and Processing of PGL/PCC and Normal Tissue Samples

A total of 145 tumor samples from 145 different patients recruited in the COMETE network from 1993 to 2008 were included in the study. Ethical approval for the study was obtained from the institutional review board (CPP Paris-Cochin, January 2007). All patients provided written informed consent for the collection of samples and subsequent analyzes. Three adrenal medulla samples from healthy individuals were also included as controls. Germline DNA was extracted from leukocytes using standard protocols. Tumor and normal medulla samples were powdered in liquid nitrogen (30–50 mg), and DNA was extracted using a QIAamp DNA Mini Kit or an AllPrep Kit (QIAGEN, Hilden, Germany). For details, see the Supplemental Experimental Procedures.

DNA Methylation Arrays

Whole-genome DNA methylation was analyzed in 145 PGL or PCC and three normal adrenal medulla samples using the Illumina Infinium HumanMethylation27 assay (Bibikova et al., 2009). Twenty-four samples were later reanalyzed using the more comprehensive Illumina Infinium HumanMethylation450 Beadchips. Microarray experiments were performed by Integragen SA (Evry, France). In brief, genomic DNA was bisulfite-converted using the EZ-96 DNA Methylation Kit (Zymo Research, Irvine, CA, USA), whole-genome amplified, enzymatically fragmented, and hybridized to the BeadChip arrays in accordance with the manufacturer's instructions. The beta value DNA methylation scores for each locus were extracted together with detection p values from Illumina GenomeStudio software. As described elsewhere (Hinoue et al., 2012), we replaced data points with a detection p value >0.05 by "NA" values, and we masked data points as "NA" for 4,484 probes that contain single-nucleotide polymorphisms or overlap with a repetitive element that are not uniquely aligned to the human genome (NCBI build 36/Hg18) or that overlap with regions of insertions and deletions in the human genome. Probes were considered to be in a promoter CpG island if they were located within a CpG island (UCSC database) and less than 1,500 bp away from a transcription start site.

DNA Methylation-Based Classification of Pheochromocytomas and Paragangliomas

We used consensus clustering (Monti et al., 2003) to identify PGL/PCC subgroups on the basis of their DNA methylation profiles. We selected the 10% most variant probes (n = 2,152) among those that did not contain any «NA»-masked data point. We then established consensus partitions of the data set in K clusters (for K = 2, 3, …, 8), based on 1,000 resampling iterations of hierarchical clustering, with Pearson's dissimilarity as the distance metric and Ward's method for linkage analysis. We used the cumulative distribution functions (CDF) of the consensus matrices to determine the optimal number of clusters, considering both the shape of the functions and the area under the CDF curves (Figure S1). The Bioconductor ConsensusClusterPlus package was used for consensus clustering analysis.

Reduced Representation Bisulphite Sequencing Analysis of Mouse Chromaffin Cells

RRBS was performed by Integragen SA (Evry, France), as described elsewhere (Gu et al., 2011; Smallwood and Kelsey, 2012). In brief, 300 ng of mouse genomic DNA were digested with 14 units of MspI (NEB). After end-repair, A-tailing, and ligation to methylated Illumina adapters, the library fragments of 40–220 bp were gel isolated, subjected to a double bisulfite conversion with the EpiTect Bisulfite kit from QIAGEN, PCR amplified, and sequenced on an Illumina HiSeq2000 sequencer as paired-end 75 bp reads. We used Trim Galore! (http://www.bioinformatics.babraham.ac.uk/projects/trim_galore) to filter out the adaptor sequences. Bisulfite mapping and methylation calling were performed in a single step using the bismark software (Krueger and Andrews, 2011). Only reads uniquely aligned to the mm9 assembly of the mouse genome were retained, and we required a coverage of at least ten reads to call methylation score for a CpG site. We downloaded the list of Mouse CpG islands from the UCSC genome browser, and we inferred a DNA methylation rate to each CpG island with more than ten individual CpG measurements and more than 100 total reads. To identify differentially methylated CpG sites or CpG islands, we compared the number of methylated and unmethylated observations in WT and *Sdhb*−/− cells using Fisher's exact test. CpG islands with an FDR-adjusted p value <0.05 and absolute methylation difference >5% were considered differentially methylated. Human and mouse orthologs were downloaded from the Mouse Genome Database (Eppig et al., 2012).

Generation of *Sdhb*–/– Immortalized Mouse Chromaffin Cells

Sdhb-floxed mice were generated at the Mouse Clinical Institute (Illkrich, France). A targeting vector containing *Sdhb* exon 2 flanked by LoxP sites followed by a neomycin (neo) selection cassette flanked by Frt sites (Figure 2A) was introduced into P1 (129 S2/SvPas) ES cells by electroporation. Two positive embryonic stem clones were injected into C57BL/6J blastocysts, and the resulting male chimeras gave germline transmission. These mice were mated to Flipase-expressing mice to delete the *Neo* cassette. $Sdhb^{+/lox}$ mice were intercrossed to obtain $Sdhb^{lox/lox}$ mice, and mouse chromaffin cells (mCCs) were isolated from the adrenal medulla of these $Sdhb^{lox/lox}$ as described elsewhere (Kolski-Andreaco et al., 2007). All studies were performed in accordance with the relevant guidelines of the French Ministry of Agriculture (Authorization Executive Order A751532) for scientific experimentation on animals, European Communities Council Directive, and international ethical standards. Cells were cultured at 37°C, under 5% CO_2 in a standard medium containing Dulbecco's modified Eagle's medium with glutamine and a high glucose concentration (DMEM glutaMAX, GIBCO, Life Technologies, Saint Aubin, France) supplemented with 10% fetal bovine serum (GIBCO) and 1% penicillin-streptomycin (GIBCO). The cultures remained quiescent for 6 months, after which some started to grow spontaneously from mCCs clusters. These immortalized cells were isolated and infected with 10^7 plaque-forming units (pfu)/ml of an adenovirus expressing Cre-recombinase (Ad5CMV-Cre, Cell BioLabs, San Diego). A clonal approach by limiting dilution cloning assay was used to obtain homogenous $Sdhb^{-/-}$ immortalized mCCs clones (imCC clones 6 and 8). $Sdhb^{-/-}$ and $Sdhb^{lox/lox}$ (referred to as WT) imCCs were maintained in standard medium with or without 2.5 mM dimethyl 2-oxoglutarate (Sigma-Aldrich, St. Louis).

ACCESSION NUMBERS

Methylation array data from the 148 human samples and RRBS data from the four mouse cell lines analyzed in this study have been deposited in NCBI's Gene Expression Omnibus (http://www.ncbi.nlm.nih.gov/geo) and are accessible through the GEO series accession number GSE43298.

SUPPLEMENTAL INFORMATION

Supplemental Information includes ten tables, five figures, and Supplemental Experimental Procedures and can be found with this article online at http://dx.doi.org/10.1016/j.ccr.2013.04.018.

ACKNOWLEDGMENTS

This work is part of the "Cartes d'Identité des Tumeurs (CIT) program" funded and developed by the "Ligue Nationale contre le Cancer" (http://cit.ligue-cancer.net).

We express our gratitude to Profs. Pierre-François Plouin and Xavier Bertagna for making this work possible by creating the COMETE Network 20 years ago. We are grateful to Prof. X. Jeunemaitre for helpful discussions and continual support. We thank Dr. Juliette Hadchouel for her technical advice and the Mouse Clinical Institute for generating the $Sdhb^{+/lox}$ mouse. We thank Jacqueline Godet and Jacqueline Metral for their strong support within the CIT program. We also thank Nabila Elarouci, Dr. Rossella Libé, Prof. Cécile Badoual, and Dr. Frédérique Tissier for their help, all members of the HEGP Genetics department, and Catherine Tritscher for technical assistance. We also thank Mélanie Letexier and Maud Vandpeene from IntegraGen for their efficacy in generating methylation data. The text was edited by Alex Edelman and associates. The work leading to these results has received funding from the Agence Nationale de la Recherche (ANR 08 GENOPATH 029 MitOxy and ANR-2011-JCJC-00701 MODEOMAPP), the GIS-Institut des Maladies Rares, and the Programme Hospitalier de Recherche Clinique grant COMETE 3 (AOM 06 179). The work leading to these results has received funding from the European Union Seventh Framework Programme (FP7/2007-2013) under grant agreement number 259735.

Received: October 13, 2012
Revised: January 29, 2013
Accepted: April 20, 2013
Published: May 23, 2013

REFERENCES

Amar, L., Bertherat, J., Baudin, E., Ajzenberg, C., Bressac-de Paillerets, B., Chabre, O., Chamontin, B., Delemer, B., Giraud, S., Murat, A., et al. (2005). Genetic testing in pheochromocytoma or functional paraganglioma. J. Clin. Oncol. *23*, 8812–8818.

Amar, L., Baudin, E., Burnichon, N., Peyrard, S., Silvera, S., Bertherat, J., Bertagna, X., Schlumberger, M., Jeunemaitre, X., Gimenez-Roqueplo, A.P., and Plouin, P.F. (2007). Succinate dehydrogenase B gene mutations predict survival in patients with malignant pheochromocytomas or paragangliomas. J. Clin. Endocrinol. Metab. *92*, 3822–3828.

Baysal, B.E., Ferrell, R.E., Willett-Brozick, J.E., Lawrence, E.C., Myssiorek, D., Bosch, A., van der Mey, A., Taschner, P.E., Rubinstein, W.S., Myers, E.N., et al. (2000). Mutations in SDHD, a mitochondrial complex II gene, in hereditary paraganglioma. Science *287*, 848–851.

Bibikova, M., Le, J., Barnes, B., Saedinia-Melnyk, S., Zhou, L., Shen, R., and Gunderson, K.L. (2009). Genome-wide DNA methylation profiling using Infinium® assay. Epigenomics *1*, 177–200.

Brière, J.J., Favier, J., Bénit, P., El Ghouzzi, V., Lorenzato, A., Rabier, D., Di Renzo, M.F., Gimenez-Roqueplo, A.P., and Rustin, P. (2005). Mitochondrial succinate is instrumental for HIF1alpha nuclear translocation in SDHA-mutant fibroblasts under normoxic conditions. Hum. Mol. Genet. *14*, 3263–3269.

Burnichon, N., Vescovo, L., Amar, L., Libé, R., de Reynies, A., Venisse, A., Jouanno, E., Laurendeau, I., Parfait, B., Bertherat, J., et al. (2011). Integrative genomic analysis reveals somatic mutations in pheochromocytoma and paraganglioma. Hum. Mol. Genet. *20*, 3974–3985.

Burnichon, N., Buffet, A., Parfait, B., Letouzé, E., Laurendeau, I., Loriot, C., Pasmant, E., Abermil, N., Valeyrie-Allanore, L., Bertherat, J., et al. (2012a). Somatic NF1 inactivation is a frequent event in sporadic pheochromocytoma. Hum. Mol. Genet. *21*, 5397–5405.

Burnichon, N., Cascón, A., Schiavi, F., Morales, N.P., Comino-Méndez, I., Abermil, N., Inglada-Pérez, L., de Cubas, A.A., Amar, L., Barontini, M., et al. (2012b). MAX mutations cause hereditary and sporadic pheochromocytoma and paraganglioma. Clin. Cancer Res. *18*, 2828–2837.

Cedar, H., and Bergman, Y. (2009). Linking DNA methylation and histone modification: patterns and paradigms. Nat. Rev. Genet. *10*, 295–304.

Dahia, P.L., Ross, K.N., Wright, M.E., Hayashida, C.Y., Santagata, S., Barontini, M., Kung, A.L., Sanso, G., Powers, J.F., Tischler, A.S., et al. (2005). A HIF1alpha regulatory loop links hypoxia and mitochondrial signals in pheochromocytomas. PLoS Genet. *1*, 72–80.

deS Senanayake, P., Denker, J., Bravo, E.L., and Graham, R.M. (1995). Production, characterization, and expression of neuropeptide Y by human pheochromocytoma. J. Clin. Invest. *96*, 2503–2509.

Eisenhofer, G., Walther, M.M., Huynh, T.T., Li, S.T., Bornstein, S.R., Vortmeyer, A., Mannelli, M., Goldstein, D.S., Linehan, W.M., Lenders, J.W., and Pacak, K. (2001). Pheochromocytomas in von Hippel-Lindau syndrome and multiple endocrine neoplasia type 2 display distinct biochemical and clinical phenotypes. J. Clin. Endocrinol. Metab. *86*, 1999–2008.

Eisenhofer, G., Pacak, K., Huynh, T.T., Qin, N., Bratslavsky, G., Linehan, W.M., Mannelli, M., Friberg, P., Grebe, S.K., Timmers, H.J., et al. (2011). Catecholamine metabolomic and secretory phenotypes in phaeochromocytoma. Endocr. Relat. Cancer *18*, 97–111.

Eppig, J.T., Blake, J.A., Bult, C.J., Kadin, J.A., and Richardson, J.E.; Mouse Genome Database Group. (2012). The Mouse Genome Database (MGD): comprehensive resource for genetics and genomics of the laboratory mouse. Nucleic Acids Res. *40*(Database issue), D881–D886.

Esteller, M., Guo, M., Moreno, V., Peinado, M.A., Capella, G., Galm, O., Baylin, S.B., and Herman, J.G. (2002). Hypermethylation-associated inactivation of the cellular retinol-binding-protein 1 gene in human cancer. Cancer Res. *62*, 5902–5905.

Farias, E.F., Ong, D.E., Ghyselinck, N.B., Nakajo, S., Kuppumbatti, Y.S., and Mira y Lopez, R. (2005). Cellular retinol-binding protein I, a regulator of breast epithelial retinoic acid receptor activity, cell differentiation, and tumorigenicity. J. Natl. Cancer Inst. *97*, 21–29.

Favier, J., Brière, J.J., Burnichon, N., Rivière, J., Vescovo, L., Benit, P., Giscos-Douriez, I., De Reyniès, A., Bertherat, J., Badoual, C., et al. (2009). The Warburg effect is genetically determined in inherited pheochromocytomas. PLoS ONE *4*, e7094.

Favier, J., Buffet, A., and Gimenez-Roqueplo, A.P. (2012). HIF2A mutations in paraganglioma with polycythemia. N. Engl. J. Med. *367*, 2161, author reply 2161–2162.

Feinberg, A.P., and Vogelstein, B. (1983). Hypomethylation distinguishes genes of some human cancers from their normal counterparts. Nature *301*, 89–92.

Geli, J., Kiss, N., Karimi, M., Lee, J.J., Bäckdahl, M., Ekström, T.J., and Larsson, C. (2008). Global and regional CpG methylation in pheochromocytomas and abdominal paragangliomas: association to malignant behavior. Clin. Cancer Res. *14*, 2551–2559.

Gimenez-Roqueplo, A.P., Dahia, P.L., and Robledo, M. (2012). An update on the genetics of paraganglioma, pheochromocytoma, and associated hereditary syndromes. Horm. Metab. Res. *44*, 328–333.

Gimenez-Roqueplo, A.P., Favier, J., Rustin, P., Mourad, J.J., Plouin, P.F., Corvol, P., Rötig, A., and Jeunemaitre, X. (2001). The R22X mutation of the SDHD gene in hereditary paraganglioma abolishes the enzymatic activity of complex II in the mitochondrial respiratory chain and activates the hypoxia pathway. Am. J. Hum. Genet. *69*, 1186–1197.

Gimenez-Roqueplo, A.P., Favier, J., Rustin, P., Rieubland, C., Crespin, M., Nau, V., Khau Van Kien, P., Corvol, P., Plouin, P.F., and Jeunemaitre, X.; COMETE Network. (2003). Mutations in the SDHB gene are associated with extra-adrenal and/or malignant phaeochromocytomas. Cancer Res. *63*, 5615–5621.

Gu, H., Smith, Z.D., Bock, C., Boyle, P., Gnirke, A., and Meissner, A. (2011). Preparation of reduced representation bisulfite sequencing libraries for genome-scale DNA methylation profiling. Nat. Protoc. *6*, 468–481.

Hanahan, D., and Weinberg, R.A. (2011). Hallmarks of cancer: the next generation. Cell *144*, 646–674.

Hinoue, T., Weisenberger, D.J., Lange, C.P., Shen, H., Byun, H.M., Van Den Berg, D., Malik, S., Pan, F., Noushmehr, H., van Dijk, C.M., et al. (2012). Genome-scale analysis of aberrant DNA methylation in colorectal cancer. Genome Res. *22*, 271–282.

Houseman, E.A., Christensen, B.C., Yeh, R.F., Marsit, C.J., Karagas, M.R., Wrensch, M., Nelson, H.H., Wiemels, J., Zheng, S., Wiencke, J.K., and Kelsey, K.T. (2008). Model-based clustering of DNA methylation array data: a recursive-partitioning algorithm for high-dimensional data arising as a mixture of beta distributions. BMC Bioinformatics *9*, 365.

Janeway, K.A., Kim, S.Y., Lodish, M., Nosé, V., Rustin, P., Gaal, J., Dahia, P.L., Liegl, B., Ball, E.R., Raygada, M., et al.; NIH Pediatric and Wild-Type GIST Clinic. (2011). Defects in succinate dehydrogenase in gastrointestinal stromal tumors lacking KIT and PDGFRA mutations. Proc. Natl. Acad. Sci. USA *108*, 314–318.

Jones, P.A., and Baylin, S.B. (2007). The epigenomics of cancer. Cell *128*, 683–692.

Kolski-Andreaco, A., Cai, H., Currle, D.S., Chandy, K.G., and Chow, R.H. (2007). Mouse adrenal chromaffin cell isolation. J. Vis. Exp. *2007 Jan 5*, 129.

Krueger, F., and Andrews, S.R. (2011). Bismark: a flexible aligner and methylation caller for Bisulfite-Seq applications. Bioinformatics *27*, 1571–1572.

Laird, P.W. (2003). The power and the promise of DNA methylation markers. Nat. Rev. Cancer *3*, 253–266.

Lenders, J.W., Eisenhofer, G., Mannelli, M., and Pacak, K. (2005). Phaeochromocytoma. Lancet *366*, 665–675.

Loriot, C., Burnichon, N., Gadessaud, N., Vescovo, L., Amar, L., Libé, R., Bertherat, J., Plouin, P.F., Jeunemaitre, X., Gimenez-Roqueplo, A.P., and Favier, J. (2012). Epithelial to mesenchymal transition is activated in metastatic pheochromocytomas and paragangliomas caused by SDHB gene mutations. J. Clin. Endocrinol. Metab. *97*, E954–E962.

Meissner, A., Gnirke, A., Bell, G.W., Ramsahoye, B., Lander, E.S., and Jaenisch, R. (2005). Reduced representation bisulfite sequencing for comparative high-resolution DNA methylation analysis. Nucleic Acids Res. *33*, 5868–5877.

Monti, S., Tamayo, P., Mesirov, J.P., and Golub, T.R. (2003). Consensus clustering. A resampling-based method for class discovery and visualization of gene-expression microarray data. Mach. Learn. *52*, 91–118.

Moreno-Bueno, G., Cubillo, E., Sarrió, D., Peinado, H., Rodríguez-Pinilla, S.M., Villa, S., Bolós, V., Jordá, M., Fabra, A., Portillo, F., et al. (2006). Genetic profiling of epithelial cells expressing E-cadherin repressors reveals a distinct role for Snail, Slug, and E47 factors in epithelial-mesenchymal transition. Cancer Res. *66*, 9543–9556.

Neumann, H.P., Bausch, B., McWhinney, S.R., Bender, B.U., Gimm, O., Franke, G., Schipper, J., Klisch, J., Altehoefer, C., Zerres, K., et al.; Freiburg-Warsaw-Columbus Pheochromocytoma Study Group. (2002). Germ-line mutations in nonsyndromic pheochromocytoma. N. Engl. J. Med. *346*, 1459–1466.

Noushmehr, H., Weisenberger, D.J., Diefes, K., Phillips, H.S., Pujara, K., Berman, B.P., Pan, F., Pelloski, C.E., Sulman, E.P., Bhat, K.P., et al.; Cancer Genome Atlas Research Network. (2010). Identification of a CpG island methylator phenotype that defines a distinct subgroup of glioma. Cancer Cell *17*, 510–522.

Pasini, B., and Stratakis, C.A. (2009). SDH mutations in tumorigenesis and inherited endocrine tumours: lesson from the phaeochromocytoma-paraganglioma syndromes. J. Intern. Med. *266*, 19–42.

Pencheva, N., Tran, H., Buss, C., Huh, D., Drobnjak, M., Busam, K., and Tavazoie, S.F. (2012). Convergent multi-miRNA targeting of ApoE drives LRP1/LRP8-dependent melanoma metastasis and angiogenesis. Cell *151*, 1068–1082.

Pollard, P.J., Brière, J.J., Alam, N.A., Barwell, J., Barclay, E., Wortham, N.C., Hunt, T., Mitchell, M., Olpin, S., Moat, S.J., et al. (2005). Accumulation of Krebs cycle intermediates and over-expression of HIF1alpha in tumours which result from germline FH and SDH mutations. Hum. Mol. Genet. *14*, 2231–2239.

Ricketts, C., Woodward, E.R., Killick, P., Morris, M.R., Astuti, D., Latif, F., and Maher, E.R. (2008). Germline SDHB mutations and familial renal cell carcinoma. J. Natl. Cancer Inst. *100*, 1260–1262.

Rodríguez-Paredes, M., and Esteller, M. (2011). Cancer epigenetics reaches mainstream oncology. Nat. Med. *17*, 330–339.

Rutter, J., Winge, D.R., and Schiffman, J.D. (2010). Succinate dehydrogenase - assembly, regulation and role in human disease. Mitochondrion *10*, 393–401.

Selak, M.A., Armour, S.M., MacKenzie, E.D., Boulahbel, H., Watson, D.G., Mansfield, K.D., Pan, Y., Simon, M.C., Thompson, C.B., and Gottlieb, E. (2005). Succinate links TCA cycle dysfunction to oncogenesis by inhibiting HIF-alpha prolyl hydroxylase. Cancer Cell *7*, 77–85.

Takai, D., and Jones, P.A. (2002). Comprehensive analysis of CpG islands in human chromosomes 21 and 22. Proc. Natl. Acad. Sci. USA *99*, 3740–3745.

Tomlinson, I.P., Alam, N.A., Rowan, A.J., Barclay, E., Jaeger, E.E., Kelsell, D., Leigh, I., Gorman, P., Lamlum, H., Rahman, S., et al.; Multiple Leiomyoma Consortium. (2002). Germline mutations in FH predispose to dominantly inherited uterine fibroids, skin leiomyomata and papillary renal cell cancer. Nat. Genet. *30*, 406–410.

Toyota, M., Ahuja, N., Ohe-Toyota, M., Herman, J.G., Baylin, S.B., and Issa, J.P. (1999). CpG island methylator phenotype in colorectal cancer. Proc. Natl. Acad. Sci. USA *96*, 8681–8686.

Tsai, H.C., Li, H., Van Neste, L., Cai, Y., Robert, C., Rassool, F.V., Shin, J.J., Harbom, K.M., Beaty, R., Pappou, E., et al. (2012). Transient low doses of DNA-demethylating agents exert durable antitumor effects on hematological and epithelial tumor cells. Cancer Cell *21*, 430–446.

van Nederveen, F.H., Gaal, J., Favier, J., Korpershoek, E., Oldenburg, R.A., de Bruyn, E.M., Sleddens, H.F., Derkx, P., Rivière, J., Dannenberg, H., et al. (2009). An immunohistochemical procedure to detect patients with paraganglioma and phaeochromocytoma with germline SDHB, SDHC, or SDHD gene mutations: a retrospective and prospective analysis. Lancet Oncol. *10*, 764–771.

Smallwood, S.A., and Kelsey, G. (2012). Genome-wide analysis of DNA methylation in low cell numbers by reduced representation bisulfite sequencing. Methods Mol. Biol. *925*, 187–197.

Ward, P.S., and Thompson, C.B. (2012). Metabolic reprogramming: a cancer hallmark even warburg did not anticipate. Cancer Cell *21*, 297–308.

Widschwendter, M., Fiegl, H., Egle, D., Mueller-Holzner, E., Spizzo, G., Marth, C., Weisenberger, D.J., Campan, M., Young, J., Jacobs, I., and Laird, P.W. (2007). Epigenetic stem cell signature in cancer. Nat. Genet. *39*, 157–158.

Xiao, M., Yang, H., Xu, W., Ma, S., Lin, H., Zhu, H., Liu, L., Liu, Y., Yang, C., Xu, Y., et al. (2012). Inhibition of α-KG-dependent histone and DNA demethylases by fumarate and succinate that are accumulated in mutations of FH and SDH tumor suppressors. Genes Dev. *26*, 1326–1338.

Xu, W., Yang, H., Liu, Y., Yang, Y., Wang, P., Kim, S.H., Ito, S., Yang, C., Wang, P., Xiao, M.T., et al. (2011). Oncometabolite 2-hydroxyglutarate is a competitive inhibitor of α-ketoglutarate-dependent dioxygenases. Cancer Cell *19*, 17–30.

Young, R.M., and Simon, M.C. (2012). Untuning the tumor metabolic machine: HIF-α: pro- and antitumorigenic? Nat. Med. *18*, 1024–1025.